Journal of Earth Science, *Vol. 30*, *No. 2*, *p. 244–257*, *April 2019* *ISSN 1674-487X*
Printed in China
https://doi.org/10.1007/s12583-018-0884-3

Conodonts and Carbon Isotopes during the Permian-Triassic Transition on the Napo Platform, South China

Yan Chen[1, 2], **Qian Ye**[1, 2, 4], **Haishui Jiang***[1, 2], **Paul B. Wignall**[3], **Jinling Yuan**[1, 2]
1. *State Key Laboratory of Biogeology and Environment Geology*, *China University of Geosciences*, *Wuhan* 430074, *China*
2. *School of Earth Sciences*, *China University of Geosciences*, *Wuhan* 430074, *China*
3. *School of Earth and Environment*, *University of Leeds*, *Leeds LS*2 9*JT*, *UK*
4. *Non-ferrous Metals Geological Exploration Bureau of Zhejiang Province*, *Shaoxing* 312000, *China*
Yan Chen: https://orcid.org/0000-0002-1606-6755; Haishui Jiang: https://orcid.org/0000-0001-9636-0307

ABSTRACT: Two Permian-Triassic boundary (PTB) sections (Pojue and Dala) are well exposed in an isolated carbonate platform (Napo Platform) on the southwestern margin of the Nanpanjiang Basin, South China. These sections provide an insight into the transition across the PTB and a detailed investigation of the conodont biostratigraphy and inorganic carbon isotopes is presented. The PTB at the Pojue Section is placed at the base of Bed 10B (a dolomitized mudstone found below a microbialite horizon), defined by the first occurrence of *Hindeodus parvus*. At the Dala Section, four conodont zones occur. They are, in ascending order, the *Hindeodus parvus* Zone, *Isarcicella staeschei* Zone, *Isarcicella isarcica* Zone and *Clarkina planata* Zone. Comparison with the Pojue Section suggests the PTB at Dala also occurs at the base of dolomitized mudstone below a microbialite horizon, although the first occurrence of *Hindeodus parvus* is near the top of a microbialite bed: an occurrence that is also seen in other platform sections. The succeeding microbialite beds developed during the ongoing PTB mass extinction phase. This time was characterized by low carbon isotope values, and a microbialite ecosystem that provided a refuge for selected groups (bivalves, ostracods and microgastropods) that were likely tolerant of extremely high temperatures.
KEY WORDS: Permian-Triassic, Napo Platform, conodont biostratigraphy, carbon isotope.

0 INTRODUCTION

The largest mass extinction in geological history occurred around the Permian-Triassic boundary (PTB). It has been studied for several decades and various extinction patterns (e.g., Shen et al., 2018, 2011; Jiang et al., 2015; Wignall, 2015; Wang et al., 2014; Song et al., 2013; Yin et al., 2012) noted with numerous causes (e.g., Sun et al., 2018; Baresel et al., 2017; Ernst and Youbi, 2017; Foster et al., 2017; Brand et al., 2016; Chen B et al., 2016; Grasby et al., 2016; Xiang et al., 2016; Chen Z-Q et al., 2015; Clarkson et al., 2015; Jiang et al., 2015; Song et al., 2014; Yin et al., 2014; Joachimski et al., 2012; Sun et al., 2012) proposed, but debate on the timing and nature of the crisis continues. Much of this discussion has been focused on sections in South China, notably the Global Stratotype Section and Point (GSSP) at Meishan and the auxiliary GSSP at Shangsi. Many sections in the Nanpanjiang Basin area have also provided important insights into PTB events, e.g., the persistence of siliceous deposition into the Early Triassic at Gaimao (Yang et al., 2012), the occurrence of delayed extinction in the deep-water location of Bianyang (Jiang et al., 2015) and the age of post-extinction microbialite facies following a hiatus in shallow, carbonate settings (Baresel et al., 2017; Jiang et al., 2014) at the Great Bank of Guizhou (GBG).

Like the GBG, the Napo Platform is also found within the Nanpanjiang Basin, being located near the southwestern margin (Fig. 1). We have undertaken the first study of conodont biostratigraphy and $\delta^{13}C_{carb}$ fluctuations at the Pojue and Dala sections (Fig. 1), in order to better constrain the mass extinction and environmental changes during the PTB on this little studied platform.

1 GEOLOGICAL SETTINGS AND FACIES DESCRIPTION

The Pojue Section is located at Pojue Village, Longhe Town, Napo County (Fig. 1). The Dala Section occurs about 37 km south of Pojue and is located at Dala Village, Nanpo Town, Jingxi County (Fig. 1). These two sections record carbonate-dominated marine sedimentation during the PTB interval and are well exposed and easily accessible.

The Upper Permian strata at Pojue are dominated by bioclastic packstone and algal-laminated bindstone of the Wuchiaping Formation. The former lithology has a rich biota which includes fusulinids, foraminifers, calcareous algae and ostracods (Fig. 2a). Only calcareous algae and foraminifers occur in the algal-laminated bindstone. The diverse biota indicates an open shallow-marine setting and a low to moderate high-energy environment in the Late Permian.

The Permian-Triassic transition strata of Pojue consist of

*Corresponding author: jiangliuis@163.com

Manuscript received October 15, 2018.
Manuscript accepted November 12, 2018.

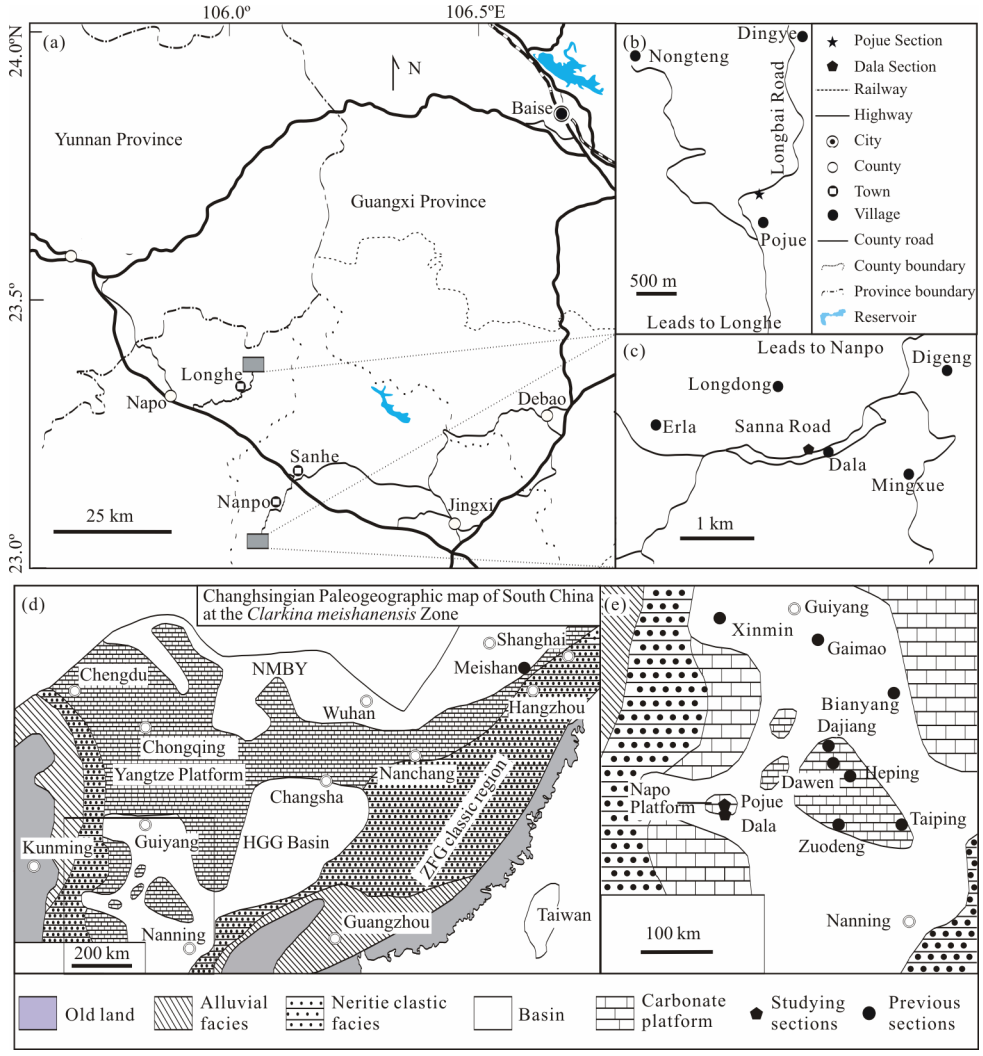

Figure 1. Location of the study sections (a)–(c) and Changhsingian paleogeographic map of South China during the Latest Permian *Clarkina meishanensis* Zone (d)–(e) (revised after Yin et al., 2014). NMBY. North marginal basin of Yangtze Platform; HGG Basin. Hunan-Guizhou-Guangxi Basin; ZFG clastic region. Zhejiang-Fujian-Guangdong clastic region.

an 8 cm-thick limestone bed (Fig. 2a), which occurs above the algal-laminated bindstone and is overlain by microbialite. It consists of dolomitized mudstone (Bed 10B, Fig. 2d), foraminiferal cortoid grainstone (Bed 10A, Fig. 2d) and stromatolites with wavy laminae. These lithologies occur as multiple distinct units bounded by uneven or irregular trunction surface shown in Fig. 2b. The lowest Triassic bed is a dolomitized mudstone that only yields *H. parvus*. It is bounded by truncation surfaces and is overlain by microbialite (Fig. 2b). The dolomite crystals are dirty with inclusions (Fig. 2d, Bed 10B).

Lower Triassic limestones sit on a truncation surface (Fig. 2e) at the top of the dolomitized mudstone (Bed 10B) mentioned above or the stromatolites (Bed 10C) from the Permian-Triassic transition bed. The 6 m-thick, calcimicrobial framestone is composed of thrombolites (characterized by clotted structures), showing occasional domal structures (Fig. 2e). This is in turn overlain by thin-bedded micritic mudstone with ostracods and conodonts. Horizontal bioturbation and thin-shelled fossils are seen in other Earliest Triassic thin-bedded strata around this level (e.g., Zhao et al., 2008; Baud et al., 2007; Wignall and Hallam, 1996) but these features are absent from the Pojue strata.

The lithology of the Dala Section is similar to that of the Pojue Section, but with some minor differences. The Upper Permian Wuchiaping Formation bioclastic packstone contains fusulinids, foraminifers, calcareous algae, ostracods and echinoderms, but the absence of algal-laminated bindstone suggests a slightly deeper water setting. The Wuchiaping Formation is once again capped by a truncation surface. Thus, the Dala Section consists, in ascending order, of cortoid grainstone with fusulinids and foraminifers, dolomitized mudstone with the conodont *H. praeparvus*, a stromatolite bed and thrombolites. The thrombolites bed in turn is overlain by thin-bedded micritic mudstones that contain ostracods or some thin-shelled fossils. Thin oolitic wackstone beds, 5–10 cm thick, are interleaved with the mudstones. The ooids, 1–2 mm in diameter, are partly recrystallized (Fig. 2f), although some show more than one nucleus and a thick cortex with irregular overlapping micritic laminae reminiscent of oncoids (Fig. 2f). Ooids also occur in GBG sections but as thicker beds of oolitic grainstone (e.g., Li et al., 2015, 2013; Tian et al., 2015; Lehrmann et al., 2012). The co-occurrence of ooids, typically produced in agitated conditions and micrite, suggesting quiet energy, at Dala implies the ooids may have formed in shallower waters and then been

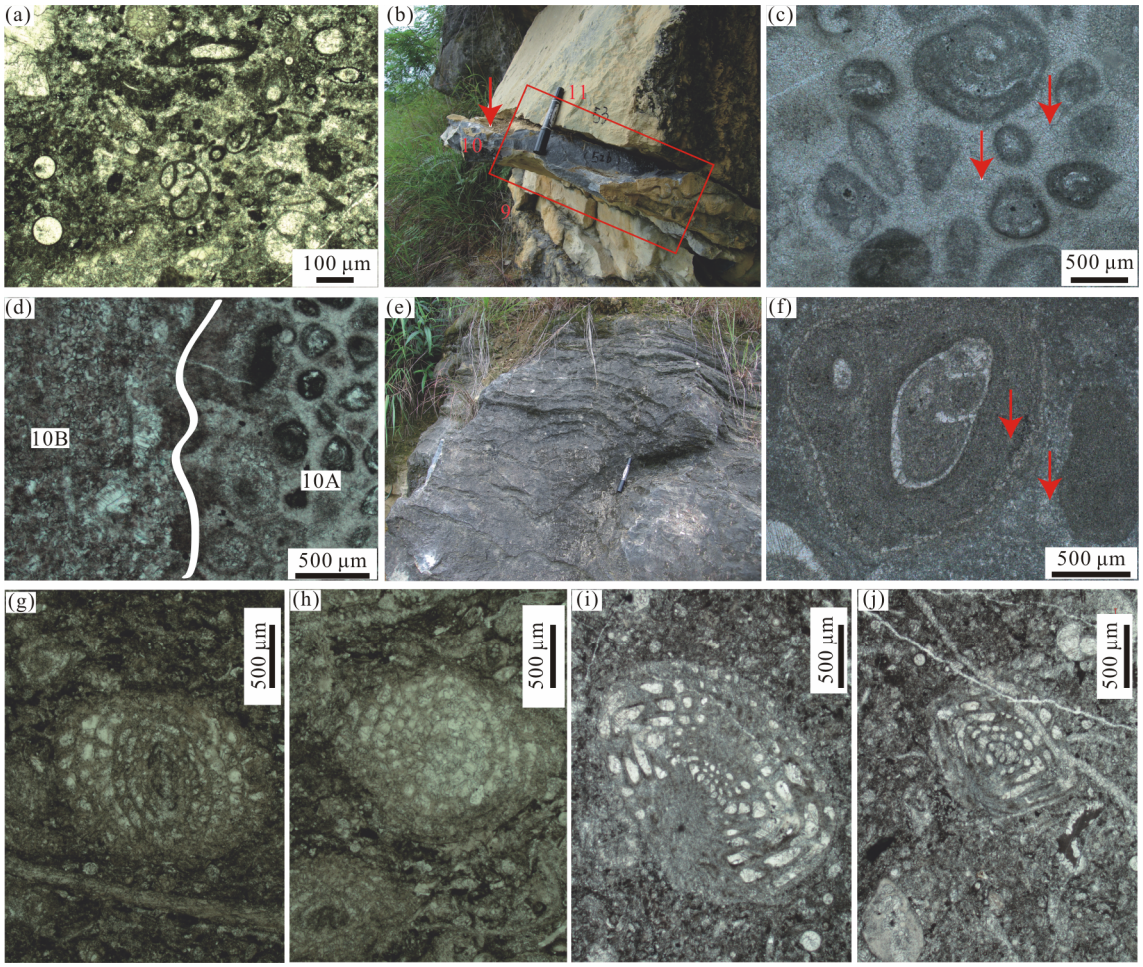

Figure 2. Outcrop and thin section photographs of Permian-Triassic boundary strata at the Pojue Section and foraminifer at the Pojue and Dala sections. (a) Bioclastic packstone at Pojue, Bed 1; (b) outcrop view of PTB at the Pojue Section, red arrow shows the dolomitized mudstone, a 0.15 m marker pen provides scale; (c) the cortoid grainstone of Bed 10A at Pojue, the red arrows show isopachous fibrous rims around micrite envelopes; (d) thin section photo of the uneven surface (vertical in this view) between the beds 10B and 10A at Pojue; (e) outcrop photo of calcimicrobial framestone with microbialite mound at Pojue, Bed 12, a 0.15 m maker pen provides scale; (f) thin section photo of an ooid in Bed 13 at Dala, the red arrows show both sides of the ooid have same characteristic and its inconspicuous laminate; (g)–(j) fusulinids at the Pojue and Dala sections; (g), (i), (j) *Nankinella* sp.; (h) *Pisoina* sp.; (g), (h) 2.76 m below the base of Bed 10B at Pojue; (i), (j) from Bed 7 at Dala.

transported into the depositional setting.

2 MATERIALS AND METHODS

In order to investigate the conodont biostratigraphy, 17 samples (each >4 kg in weight) were collected from the Pojue Section and 21 samples (each >4 kg) were collected from the Dala Section (Figs. 3 and 5). All samples were broken into fragments then dissolved in dilute acetic acid (10%) and a 2.80–2.82 g/mL heavy liquid solution (solution of lithium heteropolytungstates in water) was used to separate the conodonts from the residues (method see Yuan et al., 2015). In total 2 626 conodont elements belonging to *Hindeodus*, *Isarcicella* and *Clarkina* were obtained. Among them were 29 well preserved P_1 elements from Pojue and 322 well-preserved P_1 elements from Dala (Fig. 3).

These materials (Plates 1–4) enabled the biostratigraphy of the two sections to be evaluated.

Both the Pojue and the Dala sections of the Napo Platform in Guangxi Province have been sampled for carbon and oxygen stable isotope investigation. Bulk rock carbonates were sampled by micro drill to produce 2–4 mg powders and $^{13}C/^{12}C$ and $^{18}O/^{16}O$ ratios of CO_2 were generated by the acid reaction and measurement on a Finnigan MAT-253 at the State Key Laboratory of Biogeology and Environment Geology in Wuhan and converted to $\delta^{13}C_{carb}$ (VPDB) and $\delta^{18}O$ (VPDB) (VPDB, Vienna Pee Dee Belemnite) (Fig. 4).

3 RESULTS

3.1 Conodont Biostratigraphy

3.1.1 The Pojue Section

We failed to obtain any conodonts from beds 1 to 10A in our collections. However, abundant fusulinids and foraminifera are seen in thin section such as the fusulinids *Nankinella* sp. and *Pisoina* sp. (Figs. 2g and 2h). In addition, the fusulinids, *Sphaerulina* and the coral *Liangshanophyllum* have also been reported from these beds at Pojue, and *Palaeofusulina* and *Codonofusiella* are known from the same level regionally and indicate a Late Permian (Changhsingian) age (Regional Geological Survey Team of the Guangxi Zhuang Autonomous Region Geological Bureau, 1974).

Sections	Beds No.	Samples No.	Lithologic information	*H. parvus*	*H.* cf. *parvus*	*H. praeparvus*	*H. inflatus*	*H. peculiaris*	*I. inflata*	*I. staeschei*	*I. isarcica*	*I. prisca*	*I. turgida*	*C. carinata*	*C. lehrmanni*	*C. taylorae*	*C. planata*
Pojue	10b	PJC-09	DM	3	3	6											
	10c	PJC-10	DM	2	2	3											
	13	PJC-14	TBM	2		2											
	13	PJC-15	TBM	1													
	13	PJC-16	TBM	2		3											
Dala	9	DAL-2B	DM			3											
	10	DAL-6	CF		1	2											
	11	DAL-11	CF	2		2											
	11	DAL-12	CF	3		2				1			1				
	12	DAL-13	TBM	14		13		5		26	1						
	15	DAL-14	TBM	24		14			4	11							
	17	DAL-15	TBM	50		66	3	11				8	11	1	2	1	1
	17	DAL-16	TBM	9		14											
	17	DAL-17	TBM	2		3							3				
	17	DAL-18	TBM	1		2						2					
	17	DAL-19	TBM	1													

Figure 3. Numerical distribution of conodont species at Dala and Pojue sections, Napo and Jingxi counties, Guangxi Province. Abbreviations of the genus of conodont and lithologic information: *H.*, *Hindeodus*; *C.*, *Clarkina*; *I.*, *Isarcicella*; P1, conodont element; DM, dolomitized mudstone; TBM, thin-bedded mudstone; CF, calcimicrobial framestone.

Samples No.	$\delta^{13}C$ (‰) VPDB	$\delta^{18}O$ (‰) VPDB	Samples No.	$\delta^{13}C$ (‰) VPDB	$\delta^{18}O$ (‰) VPDB	Samples No.	$\delta^{13}C$ (‰) VPDB	$\delta^{18}O$ (‰) VPDB
Pojue			PJ15-12	0.15	-8.40	DALS-6	4.04	-5.96
PJ-1	4.95	-7.37	PJ15-13	0.20	-8.11	DALS-7	3.29	-8.42
PJ-2	4.68	-6.61	PJ15-15	-0.52	-9.10	DALS-8	1.01	-7.77
PJ-3	3.14	-8.28	PJ15-17	-0.33	-7.44	DALS-10	3.95	-6.65
PJ-4	4.87	-5.83	PJ15-19	-0.04	-6.37	DALS-11	4.10	-7.25
PJ-5	5.10	-9.29	PJ15-22	-0.45	-7.39	DALS-12	1.06	-5.64
PJ-6	4.52	-7.38	PJ15-24	-0.42	-7.65	DALS-13	0.51	-5.58
PJ-7	4.74	-6.84	PJ15-26	-0.44	-6.77	DALS-14	0.20	-5.68
PJ-8	5.10	-8.21	PJ15-28	-0.29	-6.75	DALS-15	0.03	-5.29
PJ-12	4.49	-6.69	PJ-24	-0.03	-6.08	DALS-16	-0.32	-5.62
PJ-13	2.97	-6.65	PJ15-30	-0.56	-8.19	DALS-17	-0.01	-4.98
PJ-14	3.19	-5.76	PJ15-32	-0.53	-6.51	DALS-18	0.34	-4.95
PJ-15	3.19	-7.37	PJS-1	1.77	-6.81	DALS-19	-0.39	-5.52
PJ-18	2.98	-6.51	PJS-2	2.06	-7.01	DALS-20	-0.34	-6.19
PJ-19	2.98	-5.50	PJS-3	1.96	-6.15	DALS-21	-0.54	-5.33
PJ-20	1.75	-5.91	PJS-4	1.93	-6.69	DALS-22	0.00	-6.75
PJ15-1	1.42	-6.98	PJS-5	1.91	-5.99	DALS-23	0.13	-5.9
PJ15-2	1.73	-6.09	PJS-6	2.00	-5.44	DALS-24	-0.19	-7.35
PJ-21	0.05	-8.40	PJS-7	2.16	-5.98	DALS-26	-0.23	-6.3
PJ15-3	2.24	-3.08	Dala			DALS-27	1.03	-5.59
PJ15-4	1.72	-5.98	DALS-1	4.04	-8.45	DALS-28	1.23	-6.49
PJ15-6	0.96	-6.13	DALS-2	3.35	-6.94	DALS-29	1.38	-5.49
PJ15-8	-0.09	-7.92	DALS-3	3.48	-5.35	DALS-30	1.19	-5.71
PJ15-10	-1.02	-7.70	DALS-4	3.48	-5.3	DALS-31	1.67	-7.3
PJ-23	-0.41	-7.12	DALS-5	3.76	-6.1			

Figure 4. Carbon and oxygen ratios of carbonate from Pojue and Dala sections, analyzed using MAT 253 in the State Key Laboratory of Biogeology and Environmental Geology, Wuhan, China.

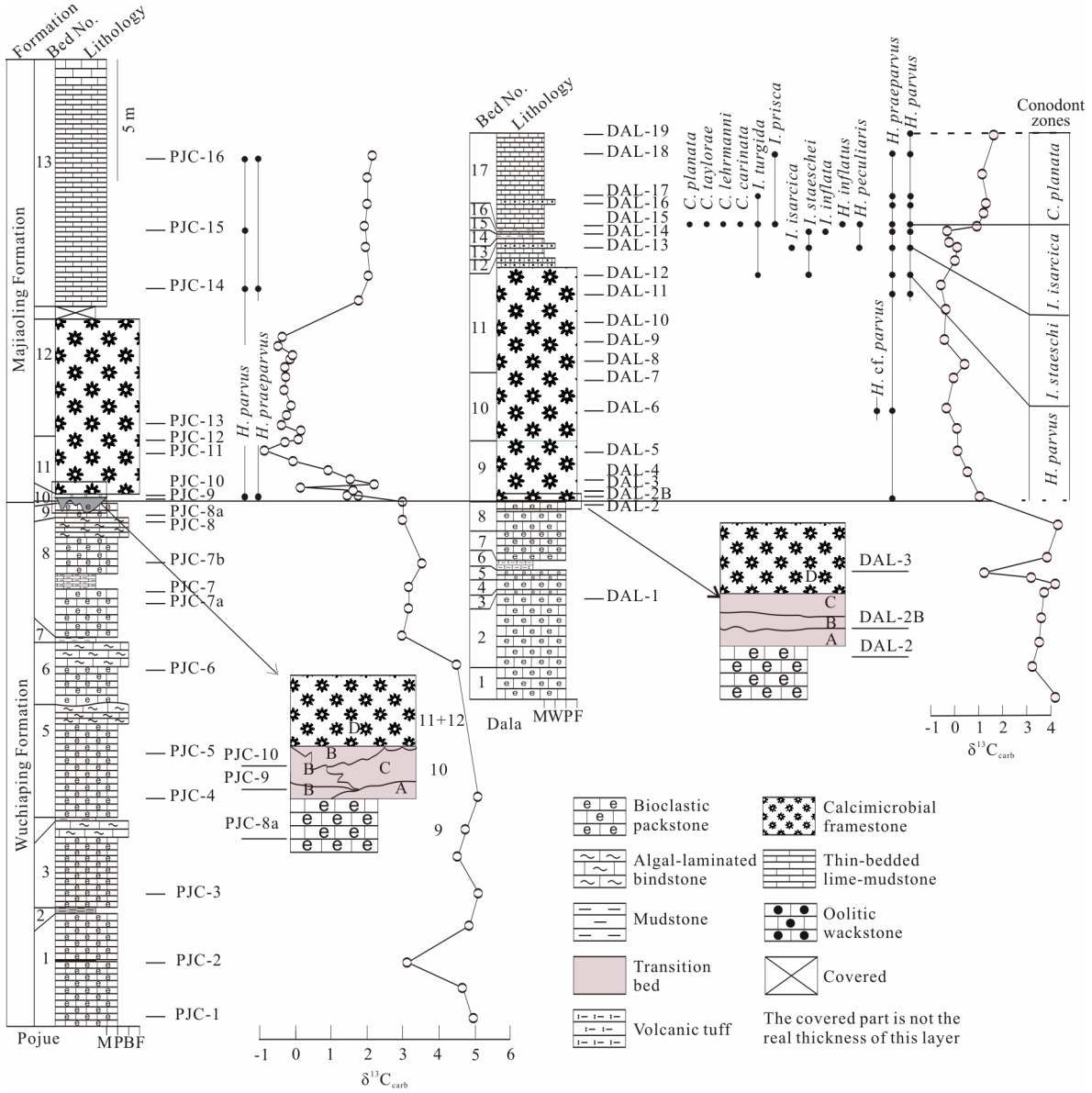

Figure 5. Lithostratigraphic logs, conodont distributions and carbon isotopes at the Pojue and Dala PTB sections. The arrows show sketch illusions of interpreted contact relationship at transition strata from Permian bioclastic packstone to Triassic microbialite at Pojue and Dala sections. A. Cortoid grainstone with foraminifer; B. dolomitized mudstone; C. calcimicrobial framestone with stromatolite; D. calcimicrobial framestone with thrombolite. Abbreviations of the genus of conodont: *H.*, *Hindeodus*; *C.*, *Clarkina*; *I.*, *Isarcicella.*

Two species, *Hindeodus parvus* and *Hindeodus praeparvus* are found at Bed 10B (Fig. 5 and Plate 1). Although this is not enough to precisely identify a conodont zone, *H. parvus* marks the base of Triassic (Yin et al., 2001), and therefore the beds above Bed 10B, including the microbialite bed, at Pojue can be assigned an Early Triassic (Griesbachian) age.

3.1.2 The Dala Section

Beds 1–8 also failed to yield conodonts at the Dala Section. However, the lithostratigraphy of this interval is very similar to that at Pojue and so we also assign a Latest Permian age to these strata at Dala. The lithostratigraphic succession from the base of Bed 9 is almost the same as that from beds 10A to 10C to Bed 11 at Pojue. Fortunately, more conodonts were collected from beds 9–17 at the Dala Section, enabling the identification of four conodont zones (Plates 1–4). In ascending order, they are: *Hindeodus parvus* Zone, *Isarcicella staeschei* Zone, *Isarcicella isarcica* Zone and *Clarkina planata* Zone.

Hindeodus parvus Zone: *Hindeodus parvus* first occurred in sample DAL-11 (Fig. 5). While a specimen of *Hindeodus* cf. *parvus* is found from Bed 10 and *Hindeodus praeparvus* is found from the base of Bed 9 (Fig. 5), based on comparison with the Pojue Section, *H. parvus* could appear in the base of Bed 9 (Fig. 5) at Dala. Thus, we tentatively place the lower limit of this zone at the base of Bed 9. The upper limit is defined by the first occurrence of *Isarcicella staeschei*. Associated taxa include *Hindeodus praeparvus* and *Hindeodus* cf. *parvus*. This zone is widely reported in Nanpanjiang Basin area (e.g., Bianyang (Yan et al., 2013), Dajiang (Jiang et al., 2014), Xinmin (Zhang et al., 2014), Dawen (Chen et al., 2009; Liu et al.,

<table>
<tr><td rowspan="2">System</td><td rowspan="2">Stages</td><td>Meishan</td><td colspan="4">Nanpanjiang Basin</td></tr>
<tr><td rowspan="2">Chen Z-Q et al. 2015 (after Jiang et al., 2011, 2007; Zhang et al., 2009)</td><td>Dawen</td><td>Gaimao</td><td>Dajiang</td><td>Napo Platform</td></tr>
<tr><td>Chen J et al. (2009); Liu et al. (2007)</td><td>Yang et al. (2012)</td><td>Jiang et al. (2014)</td><td>This paper</td></tr>
<tr><td rowspan="8">Early Triassic</td><td rowspan="8">Induan</td><td>Nc. discreta</td><td rowspan="3"></td><td>Ns. dieneri</td><td rowspan="3"></td><td rowspan="3"></td></tr>
<tr><td>C. krystyni</td></tr>
<tr><td>C. planata</td><td>C. planata</td><td>H. sosioensis</td><td>C. planata</td></tr>
<tr><td>I. isarcica</td><td>I. isarcica</td><td>I. isarcica</td><td rowspan="2">I. isarcica</td><td>I. isarcica</td></tr>
<tr><td>I. staeschei</td><td>I. staeschei</td><td rowspan="4"></td><td>I. staeschei</td></tr>
<tr><td rowspan="2">H. parvus</td><td rowspan="2">H. parvus</td><td>I. lobata</td><td rowspan="2">H. parvus</td></tr>
<tr><td>H. parvus</td></tr>
<tr><td rowspan="3">Late Permian</td><td rowspan="3">Changhsingian</td><td>C. taylorae</td><td rowspan="3"></td><td rowspan="3" colspan="3"></td></tr>
<tr><td>H. changxingensis</td></tr>
<tr><td>C. meishanensis</td></tr>
</table>

Figure 6. Correlation of the Permian-Triassic conodont zones in selected sections from South China. Abbreviations of the genus of conodont: *H.*, *Hindeodus*; *C.*, *Clarkina*; *I.*, *Isarcicella*; *Nc.*, *Neoclarkina*; *Ns.*, *Neospathodus*.

2007) and Langpai (Ezaki et al., 2008)).

Isarcicella staeschei Zone: Lower limit: first occurrence of *Isarcicella staeschei*; upper limit: first occurrence of *Isarcicella isarcica*. This zone ranges from the base of sample DAL-12 to the base of sample DAL-13 (Fig. 5). Associated taxa: *Hindeodus parvus*, *Hindeodus praeparvus* and *Isarcicella turgida*. The *I. staeschei* Zone also has been widely reported in Nanpanjiang Basin (e.g., Dawen (Chen et al., 2009; Liu et al., 2007), Langpai (Ezaki et al., 2008) and Heping (Krull et al., 2004; Lehrmann et al., 2003)).

Isarcicella isarcica Zone: Lower limit: first occurrence of *Isarcicella isarcica*; upper limit: first occurrence of *Clarkina planata*. Associated taxa: *H. parvus*, *H. praeparvus*, *H. peculiaris*, *I. staeschei*, *I. inflata* and *I. turgida*. This zone ranges from the base of sample DAL-13 to the base of sample DAL-15 in the Dala Section (Fig. 5). The zone is widely reported from the Nanpanjiang Basin (e.g., Langpai (Ezaki et al., 2008), Dawen (Chen et al., 2009; Liu et al., 2007), Gaimao (Yang et al., 2012) and Dajiang (Jiang et al., 2014)).

Clarkina planata Zone: Lower limit: first occurrence of *Clarkina planata*. The upper limit is undefined. Associated taxa: *H. parvus*, *H. praeparvus*, *H. peculiaris*, *I. inflatus*, *I. prisca*, *I. turgida*, *C. lehrmanni*, *C. carinata* and *C. taylorae*. This zone starts from the base of sample DAL-15 (Fig. 5). Wang (1996) first established the *Clarkina planata* Zone at Meishan, where it occurs in deep-water facies, and considered that it could correspond to the upper *Isarcicella staeschei* to *Hindeodus postparvus* zones in shallower water sections. Zhang et al. (2009) defined a *Clarkina tulongensis*-*Clarkina planata* assemblage zone, based on the disappearance of *I. isarcica* and the first occurrence of *Sweetospathodus kummeli* from beds 52–72 at Meishan. Yang et al. (2012) also reported *Clarkina planata* Zone at Gaimao in the Nanpanjiang Basin and defined the first occurrence of *Clarkina planata* and *Clarkina krystyni* as its base and top, respectively. The *Clarkina planata* Zone at the Dala Section is equivalent to that at Gaimao (Yang et al., 2012).

These four conodont zones of the Napo Platform can be readily correlated with sections in the Nanpanjiang Basin area and also with the GSSP at Meishan (Fig. 6).

3.2 Carbon Isotopes

The oldest $\delta^{13}C_{carb}$ values are around +5‰ at the base of the Pojue Section and decline to +3‰ in the uppermost 5 m of the Upper Permian strata. Within the lowest Triassic microbialite bed $\delta^{13}C_{carb}$ values decline rapidly and then reach stable values between -1‰ to 0‰ in Bed 11 and Bed 12. From Bed 13 upwards the $\delta^{13}C_{carb}$ values recover to higher values around +2‰ (Fig. 5).

The $\delta^{13}C_{carb}$ values at Dala show a very similar trend to the Pojue Section. Beginning around +4‰ in the Upper Permian of the Dala Section these values remain stable, except for two lower values around 2 m from the top, before a rapid shift to light values that range from -0.5‰ to 0‰ in the microbialite bed (beds 9 to 16). From the base of Bed 17, the $\delta^{13}C_{carb}$ values return to higher values (around +1‰) again (Fig. 5).

4 DISCUSSION

4.1 The Permian-Triassic Boundary

Defined by the first occurrence of *H. parvus* from Bed 10B at the Pojue Section, the PTB of this section is placed at the uneven surface between Bed 10B (Early Triassic dolomitized mudstone) and Bed 10A (Late Permian cortoid foraminifera grainstone). This situation is closely similar to that of the GBG sections such as Dajiang where the PTB is placed at the uneven surface between Permian bioclastic packstone and Lower Triassic wackstone (Jiang et al., 2014), and Yangtze Platform section like Gaohua (Wang et al., 2016) where the PTB is also placed at the uneven surface between the Upper Permian limestone to Lower Triassic microbialite. The cause of truncation has been debated with both intense ocean acidification (Payne et al., 2007) and emergence followed by karstification being proposed (Wignall et al., 2009). Lehrmann et al. (2015) concluded that the thickness for anisopachous fibrous cements below the truncation surface is random without a

downward orientation which suggests the truncation surface has formed by submarine dissolution and it caused 30–100 kyr hiatus during the *C. meishanensis*, *H. changxingensis* and *C. taylorae* zones at Meishan (21 kyr, Wu et al., 2013). However, their evidence was refuted by Kershaw et al. (2016) who favoured physical erosion as the cause of truncation. Given the shallow-water setting of the Napo Platform sections, we consider it likely that a minor sequence boundary due to regression is seen in the studied sections.

H. parvus is absent from Bed 9 at the Dala Section, but comparing with the nearby Pojue Section (only 37 km away) and considering the similar lithological sequence and the fact that *H. pareparvus* was found at the base of dolomitized mudstone below the microbialite, we surmise that the PTB is likely to occur at the base of Bed 9 at Dala. Also, as noted above, the Permian-Triassic boundary at Dajiang has also been placed at the base of a wackstone below the microbialite, similar to Gaohua (Wang et al., 2016) and Jianzishan (Bai et al., 2017) sections. This inference is supported by the similar negative shifts seen in the $\delta^{13}C_{carb}$ curve at these two sections. The *Hindeodus changxingensis* Zone is also probably missing in these two sections (c.f., Jiang et al., 2014). This was followed by the development of the dolomitized mudstone bed and subsequently the microbialite bed during the *H. parvus* Zone. The first occurrence of *H. parvus* in some microbialite sections lead Brosse et al. (2015) to argue that this species is an unreliable marker for the base of the Triassic at the Meishan GSSP. In detail, they found that *H. parvus* first appears below *H. eurypyge* and *I. turgida* in their microbialite-bearing study section at Wuzhuan whereas *H. parvus* first appears above these species at Meishan (Jiang et al., 2007). These observations lead Brosse et al. to conclude that *H. parvus* appears "late" at Meishan. Alternatively, we note that both *H. eurypyge* and *I. turgida* are very rare at Wuzhuan—the former species is only known from a single element—indicating that they are unlikely to show a range comparable with that at Meishan. Both these species are also rare conodonts in our samples from Dala and they are absent from Pojue. Collection failure of *H. eurypyge* and *I. turgida* from microbialites is a more parsimonious interpretation of conodont distributions reported by Brosse et al. (2015).

4.2 Implications for the Mass Extinction

Shen et al. (2011) estimated that the mass extinction during the PTB lasted for almost 200 kyr and was accompanied by a negative C isotope excursion. This interval was revised down to about 60±48 kyr by Burgess et al. (2014), and shortened further to ~31±31 kyr at Penglaitan Section (Shen et al., 2018). Song et al. (2013) demonstrated that there were two pulses of extinction straddling the PTB. Wang et al. (2014) attributed Song et al.'s findings to the Signor-Lipps effect and facies-dependent occurrences and concluded that there was a single extinction phase. However, Wang et al. (2014) failed to appreciate that the Song et al.'s study placed the second phase of extinction in the Early Triassic whereas the Signor-Lipps effect is only capable of making a mass extinction appear older not younger in time. In other words, implicit in the conclusion of Wang et al. is that the PTB mass extinction is an Earliest Triassic event even though they favored a single, Latest Permian extinction event. Jiang et al. (2015) reported an End-Permian foraminifera extinction at Bianyang, a deep-water location, which was later than that seen at Meishan. In contrast, He et al. (2015) suggested the deep-water brachiopods disappeared earlier than shallow-water brachiopods. Thus, extinction patterns clearly vary in different depositional settings in South China and span from the Latest Permian to the Earliest Triassic (see also Song et al., 2014). Biostratigraphically, the maximum extinction interval ranges from Bed 24e to Bed 28 at Meishan (Shen et al., 2011) and thus started in the *C. meishanensis* Zone and ended in the *I. staeschei* Zone (Chen Z-Q et al., 2015; Jiang et al., 2007). Although the *H. changxingensis* Zone is likely absent at Dala and Pojue, these sections still record most of the PTB interval. It is interesting that the $\delta^{13}C_{carb}$ record at the two sections also shows lower values during the extinction interval (Fig. 7). This correspondence is also seen at the Dajiang Section in GBG area (Luo et al., 2010) and at many other sections such as the Meishan GSSP (Shen et al., 2013; Fig. 7). Pojue and Dajiang sections both show a single negative shift beginning at the end of the Permian and culminating in an Earliest Triassic low of about 0 to -1‰ (Yin et al., 2014). Considering the *C. meishanensis* (±*H. changxingensis*) missing zone(s) (Yin et al., 2014), the shallow platform facies sections also can be correlated with the Meishan Section through the $\delta^{13}C_{carb}$ excursion, despite only one negative excursion observed at shallow water sections. Pojue, Dala, and Dajiang (shallow water) sections have higher carbon isotope values in the extinction interval, of about 0 to -1‰, than deeper water sections like Meishan which have negative values of about -2‰ to -5‰ (Song et al., 2012).

The Permian-Triassic mass extinction was not a sudden event in South China, but a phase of progressive environmental deterioration, spanning a few hundred of thousand years, linked to rapid global warming and the widespread development of marine anoxia (e.g., Jiang et al., 2015; Song et al., 2014). The microbialites of the Napo Platform developed on carbonate platforms during the PTB extinction and represent a simple microbial ecosystem (Wang et al., 2011). The abundant microbes could have served as a major food source and also provided a local oxygen supply, thereby enhancing the hospitality of the ecosystem and providing a refuge for ostracods and other organisms, although the community lacked a well-developed trophic hierarchy (Forel et al., 2013). The organisms present in the microbialite ecosystems (bivalves, ostracods and microgastropods) belong to groups with exceptional tolerance to high temperatures (Song et al., 2014), a factor that may also have been important in their occurrence. Unusually diverse bivalve and gastropod assemblages have also been reported from the contemporary microbialites at the Shanggan Section, Leye County, Guangxi, South China (Hautmann et al., 2011). Thus, like deep-water settings, microbialites offered a temporary refuge during the PTB mass extinction.

5 CONCLUSIONS

The conodont biostratigraphy and carbon isotope record across the PTB at Pojue and Dala on the Napo Platform have been documented. Four conodont zones: *H. parvus* Zone, *I. staeschei* Zone, *I. isarcica* Zone and *C. planata* Zone are identified at Dala. Defined by the first occurrence of *H. parvus,* the PTB is placed at the base of a dolomitized bed (Bed 10B) at Pojue. Correlating, using lithofacies development and carbon

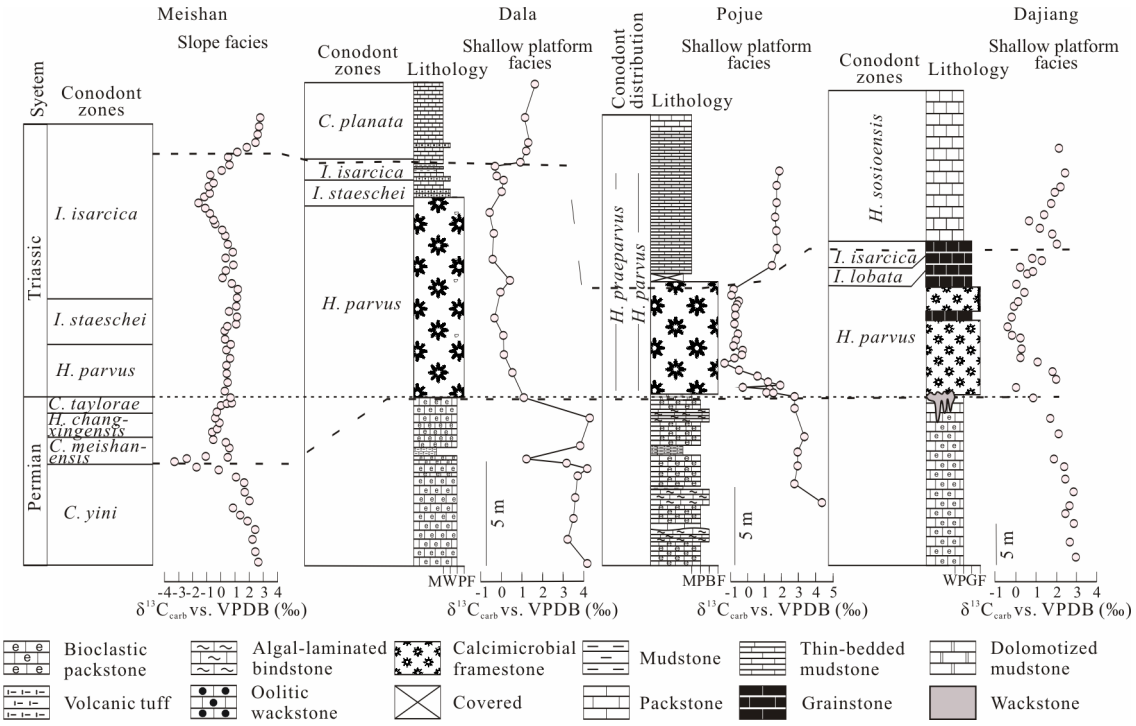

Figure 7. Correlation of $\delta^{13}C_{carb}$ carbon curve and conodont zones for Pojue, Dala, Dajiang (Jiang et al., 2014; Luo et al., 2010), and Meishan GSSP (Shen et al., 2013). Abbreviations of the genus of conodont: *H.*, *Hindeodus*; *C.*, *Clarkina*; *I. Isarcicella.*

isotope stratigraphy, the PTB at Dala is also placed at the base of a similar dolomitized bed (base of Bed 9 Fig. 5, B). The idea that *H. parvus* appears at a lower level in microbialite sections than in the Meishan Stratotype is based on the late occurrence of the rare species *H. eurypyge* and *I. turgida* in the microbialites and so we suggest that this notion is unsafe.

Both carbon isotope curves at the two sections show lower values during the mass extinction interval implying that the mass extinction was not a sudden event. The Napo Platform sections show a sequence of events that provide much detail on the cause of the mass extinction. Thus, Latest Permian times saw the development of shallow-water packstone facies with a high-diversity fauna. These strata are truncated and a hiatus spanning the *C. meishanensis* and *H. changxingensis* Zone is developed. The mass extinction began during this unrecorded interval on the Napo Platform.

ACKNOWLEDGMENTS

This work was supported by the National Natural Science Foundation of China (No. 41572324), the Special Project on Basic Work of Science and Technology from the National Ministry of Science and Technology of China (No. 2015FY310100-11), and the China Geological Survey (No. DD20160120-04). SEM pictures and carbon isotopes data were undertaken at the State Key Laboratory of Biogeology and Environmental Geology (China). We thank Suxin Zhang, Yuheng Fang for their assistance in SEM. Thanks also go to Huyue Song for the helps in processing the carbon isotopes data. The final publication is available at Springer via https://doi.org/10.1007/s12583-018-0884-3.

REFERENCES CITED

Bai, R. Y., Dai, X., Song, H. J., 2017. Conodont and Ammonoid Biostratigraphies around the Permian-Triassic Boundary from Jianzishan of South China. *Journal of Earth Science*, 28(4): 595–613. https://doi.org/10.1007/s12583-017-0754-4

Baresel, B., Bucher, H., Bagherpour, B., et al., 2017. Timing of Global Regression and Microbial Bloom Linked with the Permian-Triassic Boundary Mass Extinction: Implications for Driving Mechanisms. *Scientific Reports*, 7(1): 43630. https://doi.org/10.1038/srep43630

Baud, A., Richoz, S., Pruss, S., 2007. The Lower Triassic Anachronistic Carbonate Facies in Space and Time. *Global and Planetary Change*, 55(1/2/3): 81–89. https://doi.org/10.1016/j.gloplacha.2006.06.008

Brand, U., Blamey, N., Garbelli, C., et al., 2016. Methane Hydrate: Killer Cause of Earth's Greatest Mass Extinction. *Palaeoworld*, 25(4): 496–507. https://doi.org/10.1016/j.palwor.2016.06.002

Brosse, M., Bucher, H., Bagherpour, B., et al., 2015. Conodonts from the Early Triassic Microbialite of Guangxi (South China): Implications for the Definition of the Base of the Triassic System. *Palaeontology*, 58(3): 563–584. https://doi.org/10.1111/pala.12162

Burgess, S. D., Bowring, S., Shen, S. Z., 2014. High-Precision Timeline for Earth's Most Severe Extinction. *Proceedings of the National Academy of Sciences*, 111(9): 3316–3321. https://doi.org/10.1073/pnas.1317692111

Chen, B., Joachimski, M. M., Wang, X. D., et al., 2016. Ice Volume and Paleoclimate History of the Late Paleozoic Ice Age from Conodont Apatite Oxygen Isotopes from Naqing (Guizhou, China). *Palaeogeography, Palaeoclimatology, Palaeoecology*, 448: 151–161. https://doi.org/10.1016/j.palaeo.2016.01.002

Chen, J., Beatty, T. W., Henderson, C. M., et al., 2009. Conodont Biostratigraphy across the Permian-Triassic Boundary at the Dawen Section, Great Bank of Guizhou, Guizhou Province, South China: Implications for the Late Permian Extinction and Correlation with Meishan. *Journal of Asian Earth Sciences*, 36(6): 442–458. https://doi.org/10.1016/j.jseaes.2008.08.002

Chen, Z.-Q., Yang, H., Luo, M., et al., 2015. Complete Biotic and Sedimentary Records of the Permian-Triassic Transition from Meishan Section,

South China: Ecologically Assessing Mass Extinction and Its Aftermath. *Earth-Science Reviews*, 149: 67–107. https://doi.org/10.1016/j.earscirev.2014.10.005

Clark, D. L., 1959. Conodonts from the Triassic of Nevada and Utah. *Journal of Paleontology*, 33(2): 305–312

Clarkson, M. O., Kasemann, S. A., Wood, R. A., et al., 2015. Ocean Acidification and the Permo-Triassic Mass Extinction. *Science*, 348(6231): 229–232. https://doi.org/10.1126/science.aaa0193

Ernst, R. E., Youbi, N., 2017. How Large Igneous Provinces Affect Global Climate, sometimes Cause Mass Extinctions, and Represent Natural Markers in the Geological Record. *Palaeogeography*, *Palaeoclimatology*, *Palaeoecology*, 478: 30–52. https://doi.org/10.1016/j.palaeo.2017.03.014

Ezaki, Y., Liu, J., Nagano, T., et al., 2008. Geobiological Aspects of the Earliest Triassic Microbialites along the Southern Periphery of the Tropical Yangtze Platform: Initiation and Cessation of a Microbial Regime. *PALAIOS*, 23(6): 356–369. https://doi.org/10.2110/palo.2007.p07-035r

Forel, M. B., Crasquin, S., Kershaw, S., et al., 2013. In the Aftermath of the End-Permian Extinction: The Microbialite Refuge?. *Terra Nova*, 25(2): 137–143. https://doi.org/10.1111/ter.12017

Foster, W. J., Danise, S., Price, G. D., et al., 2017. Subsequent Biotic Crises Delayed Marine Recovery Following the Late Permian Mass Extinction Event in Northern Italy. *PLOS ONE*, 12(3): e0172321. https://doi.org/10.1371/journal.pone.0172321

Grasby, S. E., Beauchamp, B., Knies, J., 2016. Early Triassic Productivity Crises Delayed Recovery from World's Worst Mass Extinction. *Geology*, 44(9): 779–782. https://doi.org/10.1130/g38141.1

Hautmann, M., Bucher, H., Brühwiler, T., et al., 2011. An Unusually Diverse Mollusc Fauna from the Earliest Triassic of South China and Its Implications for Benthic Recovery after the End-Permian Biotic Crisis. *Geobios*, 44(1): 71–85. https://doi.org/10.1016/j.geobios.2010.07.004

He, W. H., Shi, G. R., Twitchett, R. J., et al., 2015. Late Permian Marine Ecosystem Collapse Began in Deeper Waters: Evidence from Brachiopod Diversity and Body Size Changes. *Geobiology*, 13(2): 123–138. https://doi.org/10.1111/gbi.12119

Huckriede, R., 1958. Die Conodonten Der Mediterranen Trias und Ihr Stratigraphischer Wert. *Paläontologische Zeitschrift*, 32(3/4): 141–175

Jiang, H. S., Aldridge, R. J., Lai, X. L., et al., 2011. Phylogeny of the Conodont Genera Hindeodus and Isarcicella across the Permian-Triassic Boundary. *Lethaia*, 44(4): 374–382. https://doi.org/10.1111/j.1502-3931.2010.00248.x

Jiang, H. S., Joachimski, M. M., Wignall, P. B., et al., 2015. A Delayed End-Permian Extinction in Deep-Water Locations and Its Relationship to Temperature Trends (Bianyang, Guizhou Province, South China). *Palaeogeography*, *Palaeoclimatology*, *Palaeoecology*, 440: 690–695. https://doi.org/10.1016/j.palaeo.2015.10.002

Jiang, H. S., Lai, X. L., Luo, G. M., et al., 2007. Restudy of Conodont Zonation and Evolution across the P/T Boundary at Meishan Section, Changxing, Zhejiang, China. *Global and Planetary Change*, 55(1/2/3): 39–55. https://doi.org/10.1016/j.gloplacha.2006.06.007

Jiang, H. S., Lai, X. L., Sun, Y. D., et al., 2014. Permian-Triassic Conodonts from Dajiang (Guizhou, South China) and Their Implication for the Age of Microbialite Deposition in the Aftermath of the End-Permian Mass Extinction. *Journal of Earth Science*, 25(3): 413–430. https://doi.org/10.1007/s12583-014-0444-4

Joachimski, M. M., Lai, X., Shen, S., et al., 2012. Climate Warming in the Latest Permian and the Permian-Triassic Mass Extinction. *Geology*, 40(3): 195–198. https://doi.org/10.1130/g32707.1

Kershaw, S., Collin, P. Y., Crasquin, S., 2016. Comment to Lehrmann et al. New Sections and Observations from the Nanpanjiang Basin, South China. *PALAIOS*, 31(3): 111–117. https://doi.org/10.2110/palo.2015.093

Kozur, H., 1995. Some Remarks to the Conodonts *Hindeodus* and *Isarcicella* in the Latest Permian and Earliest Triassic. *Palaeoworld*, 6: 64–77

Kozur, H., 1996. The Conodonts *Hindeodus*, *Isarcicella*, *Sweetohindeodus* in the Uppermost Permian and Lowermost Triassic. *Geologia Croatica*, 49(1): 81–116

Kozur, H., Mostler, H., Rahimi-Yazd, A., 1975. Beiträge zur Mikrofauna Permotriadischer Schichtfolgen Teil II: Neue Conodonten aus dem Oberperm und der Basalen Trias von Nord- und Zentraliran. *Geol. Palaont. Mitt. Innsbruck*, 5(3): 1–23

Kozur, H., Pjatakova, M., 1976. Die Conodontenart Anchignathodus parvus n.sp., eine wichtige Leiform der basalen Trias. *Proceedings Koninkl Nederland Akademie van Wetenschappen*, *Series B*, 79: 123–128

Krull, E. S., Lehrmann, D. J., Druke, D., et al., 2004. Stable Carbon Isotope Stratigraphy across the Permian-Triassic Boundary in Shallow Marine Carbonate Platforms, Nanpanjiang Basin, South China. *Palaeogeography*, *Palaeoclimatology*, *Palaeoecology*, 204(3/4): 297–315. https://doi.org/10.1016/s0031-0182(03)00732-6

Lehrmann, D. J., Bentz, J. M., Wood, T., et al., 2015. Environmental Controls on the Genesis of Marine Microbialites and Dissolution Surface Associated with the End-Permian Mass Extinction: New Sections and Observations from the Nanpanjiang Basin, South China. *PALAIOS*, 30(7): 529–552. https://doi.org/10.2110/palo.2014.088

Lehrmann, D. J., Minzoni, M., Li, X. W., et al., 2012. Lower Triassic Oolites of the Nanpanjiang Basin, South China: Facies Architecture, Giant Ooids, and Diagenesis—Implications for Hydrocarbon Reservoirs. *AAPG Bulletin*, 96(8): 1389–1414. https://doi.org/10.1306/01231211148

Lehrmann, D. J., Payne, J. L., Felix, S. V., et al., 2003. Permian-Triassic Boundary Sections from Shallow-Marine Carbonate Platforms of the Nanpanjiang Basin, South China: Implications for Oceanic Conditions Associated with the End-Permian Extinction and Its Aftermath. *PALAIOS*, 18(2): 138–152. https://doi.org/10.1669/0883-1351(2003)18<138:pbsfsc>2.0.co;2

Li, F., Yan, J. X., Algeo, T., et al., 2013. Paleoceanographic Conditions Following the End-Permian Mass Extinction Recorded by Giant Ooids (Moyang, South China). *Global and Planetary Change*, 105: 102–120. https://doi.org/10.1016/j.gloplacha.2011.09.009

Li, F., Yan, J. X., Chen, Z. Q., et al., 2015. Global Oolite Deposits Across the Permian-Triassic Boundary: A Synthesis and Implications for Palaeoceanography Immediately after the End-Permian Biocrisis. *Earth-Science Reviews*, 149: 163–180. https://doi.org/10.1016/j.earscirev.2014.12.006

Li, Z. S., Zhan L. P., Dai, J. Y., et al., 1989. Study on the Permian-Triassic Biostratigraphy and Event Stratigraphy of Northern Sichuan and Southern Shaanxi. Geological Memoirs Vol. 9. Geological Publishing House, Beijing. 448 (in Chinese)

Liu, J. B., Ezaki, Y., Yang, S. R., et al., 2007. Age and Sedimentology of Microbialites after the End-Permian Mass Extinction in Luodian, Guizhou Province. *Journal of Palaeogeography*, 9(5): 473–486 (in Chinese with English Abstract)

Luo, G. M., Kump, L. R., Wang, Y. B., et al., 2010. Isotopic Evidence for an Anomalously Low Oceanic Sulfate Concentration Following End-Permian Mass Extinction. *Earth and Planetary Science Letters*, 300(1/2): 101–111. https://doi.org/10.1016/j.epsl.2010.09.041

Nicoll, R. S., Metcalfe, I., Wang, C. Y., 2002. New Species of the Conodont Genus Hindeodus and the Conodont Biostratigraphy of the Permian-Triassic Boundary Interval. *Journal of Asian Earth Sciences*, 20(6): 609–631. https://doi.org/10.1016/s1367-9120(02)00021-4

Orchard, M. J., Nassichuk, W. W., Rui, L., 1994. Conodonts from the Lower

Griesbachian *Otoceras Latilobatum* Bed of Selong, Tibet and the Position of the Permian-Triassic boundary. *Memoir-Canadian Society of Petroleum Geologists*, 17: 823–843

Payne, J. L., Lehrmann, D. J., Follett, D., et al., 2007. Erosional Truncation of Uppermost Permian Shallow-Marine Carbonates and Implications for Permian-Triassic Boundary Events. *Geological Society of America Bulletin*, 119(7/8): 771–784. https://doi.org/10.1130/b26091.1

Perri, M. C., Farabegoli, F., 2003. Conodonts across the Permian-Triassic Boundary in the Southern Alps. In: Mawson, R., Talent, J. A., eds., Contributions to the Second Australian Conodont Symposium. *Courier Forschungsinstitut Senckenberg Series*, 281–313

Regional Geological Survey Team of the Guangxi Zhuang Autonomous Region Geological Bureau, 1974. 1 : 20 000 Regional Geological Survey Report of the People's Republic of China: Baise Map and Delong Map, Geological Part. Guangxi Zhuang Autonomous Region Geological Bureau, Yishan. 1–188 (in Chinese)

Shen, S. Z., Cao, C. Q., Zhang, H., et al., 2013. High-Resolution $\delta^{13}C_{carb}$ Chemostratigraphy from Latest Guadalupian through Earliest Triassic in South China and Iran. *Earth and Planetary Science Letters*, 375: 156–165. https://doi.org/10.1016/j.epsl.2013.05.020

Shen, S. Z., Crowley, J. L., Wang, Y., et al., 2011. Calibrating the End-Permian Mass Extinction. *Science*, 334(6061): 1367–1372. https://doi.org/10.1126/science.1213454

Shen, S. Z., Ramezani, J., Chen, J., et al., 2018. A Sudden End-Permian Mass Extinction in South China. *GSA Bulletin*. https://doi.org/10.1130/b31909.1

Song, H. J., Tong, J. N., Xiong, Y. L., et al., 2012. The Large Increase of $\delta^{13}C_{carb}$-Depth Gradient and the End-Permian Mass Extinction. *Science China Earth Sciences*, 55(7): 1101–1109. https://doi.org/10.1007/s11430-012-4416-1

Song, H. J., Wignall, P. B., Chu, D. L., et al., 2014. Anoxia/High Temperature Double Whammy during the Permian-Triassic Marine Crisis and Its Aftermath. *Scientific Reports*, 4(1): 4132. https://doi.org/10.1038/srep04132

Song, H. J., Wignall, P. B., Tong, J. N., et al., 2013. Two Pulses of Extinction during the Permian-Triassic Crisis. *Nature Geoscience*, 6(1): 52–56. https://doi.org/10.1038/ngeo1649

Sun, H., Xiao, Y. L., Gao, Y. J., et al., 2018. Rapid Enhancement of Chemical Weathering Recorded by Extremely Light Seawater Lithium Isotopes at the Permian-Triassic Boundary. *Proceedings of the National Academy of Sciences*, 115(15): 3782–3787. https://doi.org/10.1073/pnas.1711862115

Sun, Y. D., Joachimski, M. M., Wignall, P. B., et al., 2012. Lethally Hot Temperatures during the Early Triassic Greenhouse. *Science*, 338(6105): 366–370. https://doi.org/10.1126/science.1224126

Tian, L., Bottjer, D. J., Tong, J. N., et al., 2015. Distribution and Size Variation of Ooids in the Aftermath of the Permian-Triassic Mass Extinction. *PALAIOS*, 30(9): 714–727. https://doi.org/10.2110/palo.2014.110

Wang, C. Y., 1996. Conodont Evolutionary Lineage and Zonation for the Latest Permian and the Earliest Triassic. *Permophiles*, 29: 30–37

Wang, L. N., Wignall, P. B., Wang, Y. B., et al., 2016. Depositional Conditions and Revised Age of the Permo-Triassic Microbialites at Gaohua Section, Cili County (Hunan Province, South China). *Palaeogeography*, *Palaeoclimatology*, *Palaeoecology*, 443: 156–166. https://doi.org/10.1016/j.palaeo.2015.11.032

Wang, Y. B., Meng, Z., Liao, W., et al., 2011. Shallow Marine Ecosystem Feedback to the Permian/Triassic Mass Extinction. *Frontiers of Earth Science*, 5(1): 14–22. https://doi.org/10.1007/s11707-011-0164-3

Wang, Y., Sadler, P. M., Shen, S. Z., et al., 2014. Quantifying the Process and Abruptness of the End-Permian Mass Extinction. *Paleobiology*, 40(1): 113–129. https://doi.org/10.1666/13022

Wignall, P. B., 2015. The Worst of Times: How Life on Earth Survived Eighty Million Years of Extinctions. Princeton University Press, Princeton. 224. https://doi.org/10.1515/9781400874248

Wignall, P. B., Hallam, A., 1996. Facies Change and the End-Permian Mass Extinction in S.E. Sichuan, China. *PALAIOS*, 11(6): 587–596. https://doi.org/10.2307/3515193

Wignall, P. B., Kershaw, S., Collin, P. Y., et al., 2009. Erosional Truncation of Uppermost Permian Shallow-Marine Carbonates and Implications for Permian-Triassic Boundary Events: Comment. *Geological Society of America Bulletin*, 121(5/6): 954–956. https://doi.org/10.1130/b26424.1

Wu, H. C., Zhang, S. H., Hinnov, L. A., et al., 2013. Time-Calibrated Milankovitch Cycles for the Late Permian. *Nature Communications*, 4(1): 2452. https://doi.org/10.1038/ncomms3452

Xiang, L., Schoepfer, S. D., Zhang, H., et al., 2016. Oceanic Redox Evolution across the End-Permian Mass Extinction at Shangsi, South China. *Palaeogeography*, *Palaeoclimatology*, *Palaeoecology*, 448: 59–71. https://doi.org/10.1016/j.palaeo.2015.10.046

Yan, C. B., Wang, L. N., Jiang, H. S., et al., 2013. Uppermost Permian to Lower Triassic Conodonts at Bianyang Section, Guihzou Province, South China. *PALAIOS*, 28(8): 509–522. https://doi.org/10.2110/palo.2012.p12-077r

Yang, B., Lai, X. L., Wignall, P. B., et al., 2012. A Newly Discovered Earliest Triassic Chert at Gaimao Section, Guizhou, Southwestern China. *Palaeogeography*, *Palaeoclimatology*, *Palaeoecology*, 344/345: 69–77. https://doi.org/10.1016/j.palaeo.2012.05.019

Yin, H. F., Jiang, H. S., Xia, W. C., et al., 2014. The End-Permian Regression in South China and Its Implication on Mass Extinction. *Earth-Science Reviews*, 137: 19–33. https://doi.org/10.1016/j.earscirev.2013.06.003

Yin, H. F., Xie, S. C., Luo, G. M., et al., 2012. Two Episodes of Environmental Change at the Permian-Triassic Boundary of the GSSP Section Meishan. *Earth-Science Reviews*, 115(3): 163–172. https://doi.org/10.1016/j.earscirev.2012.08.006

Yin, H. F., Zhang, K. X., Tong, J. N., et al., 2001. The Global Stratotype Section and Point (GSSP) of the Permian-Triassic Boundary. *Episodes*, 24(2): 102–114

Yuan, J. L., Jiang, H. S., Wang, D. C., 2015. LST: A New Inorganic Heavy Liquid Used in Conodont Separation. *Geological Science and Technology Information*, 34(5): 225–230 (in Chinese with English Abstract)

Zhang, K. X., Tong, J. N., Lai, X. L., et al., 2009. Progress on Study of Conodont Sequence for the GSSP Section at Meishan, Changxing, Zhejiang Province, South China. *Acta Palaeontologica Sinica*, 48(3): 474–486 (in Chinese with English Abstract)

Zhang, N., Jiang, H. S., Zhong, W. L., et al., 2014. Conodont Biostratigraphy across the Permian-Triassic Boundary at the Xinmin Section, Guizhou, South China. *Journal of Earth Science*, 25(5): 779–786. https://doi.org/10.1007/s12583-014-0472-0

Zhao, X. M., Tong, J. N., Yao, H. Z., et al., 2008. Anachronistic Facies in the Lower Triassic of South China and Their Implications to the Ecosystems during the Recovery Time. *Science in China Series D*: *Earth Sciences*, 51(11): 1646–1657. https://doi.org/10.1007/s11430-008-0128-y

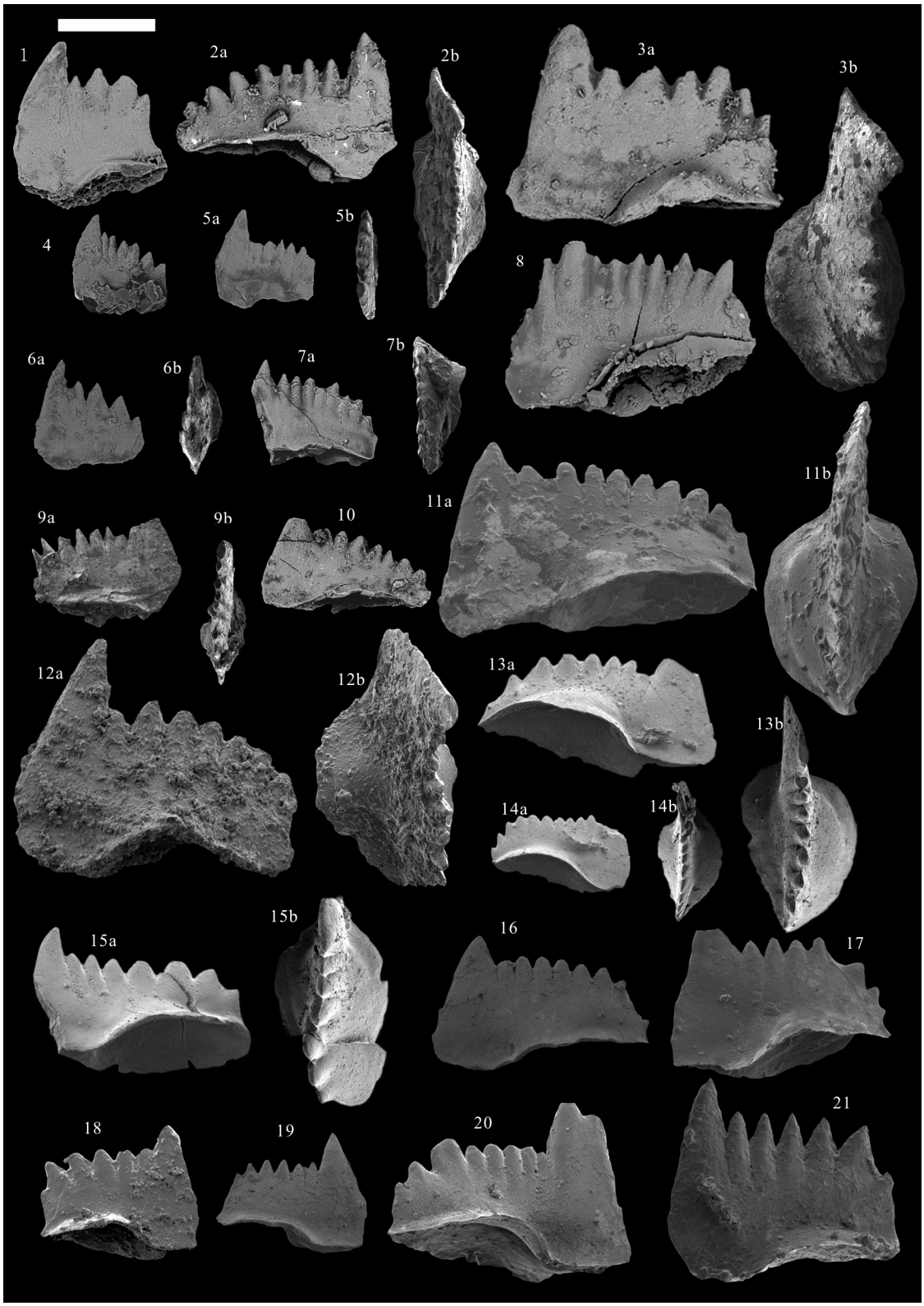

Plate 1. P_1 elements from Pojue and Dala sections. Scale bar equals 200 μm. 1–11 obtained from Pojue Section. 1, 3, 5, 9. *Hindeodus parvus* (Kozur and Pjatakova, 1976); 1. Bed 10b, PJC-09, lateral view; 3. Bed 10b, PJC-09, lateral view and upper view; 5. Bed 13, PJC-15, lateral view and upper view; 9. Bed 10b, PJC-09, lateral view and upper view. 2, 4, 6, 7, 8, 10, 11. *Hindeous praeparvus* Kozur, 1996; 2. Bed 10c, PJC-10, lateral view and upper view; 4. Bed 13, PJC-14, lateral view; 6. Bed 10b, PJC-09, lateral view and upper view; 7. Bed 13, PJC-13, lateral view and upper view; 8; Bed 13, PJC-16, lateral view; 10. Bed 10c, PJC-10, lateral view; 11. Bed 10b, PJC-09, lateral view and upper view. 12–21 obtained from Dala Section. 12, 19, 20. *Hindeodus parvus* (Kozur and Pjatakova, 1976); 12. Bed 15, DAL-14, lateral view and upper view; 19. Bed 17, DAL-16, lateral view; 20. Bed 15, DAL-14, lateral view. 13, 14, 15, 16, 18, 21. *Hindeodus praeparvus* Kozur, 1996; 13, 14, 15. Bed 9, DAL-2B, lateral view and upper view; 16. Bed 17, DAL-15, lateral view; 18, 21. Bed 17, DAL-16, lateral view. 17. *Hindeodus inflatus* (Nicoll et al., 2002); Bed 17, DAL-15, lateral view.

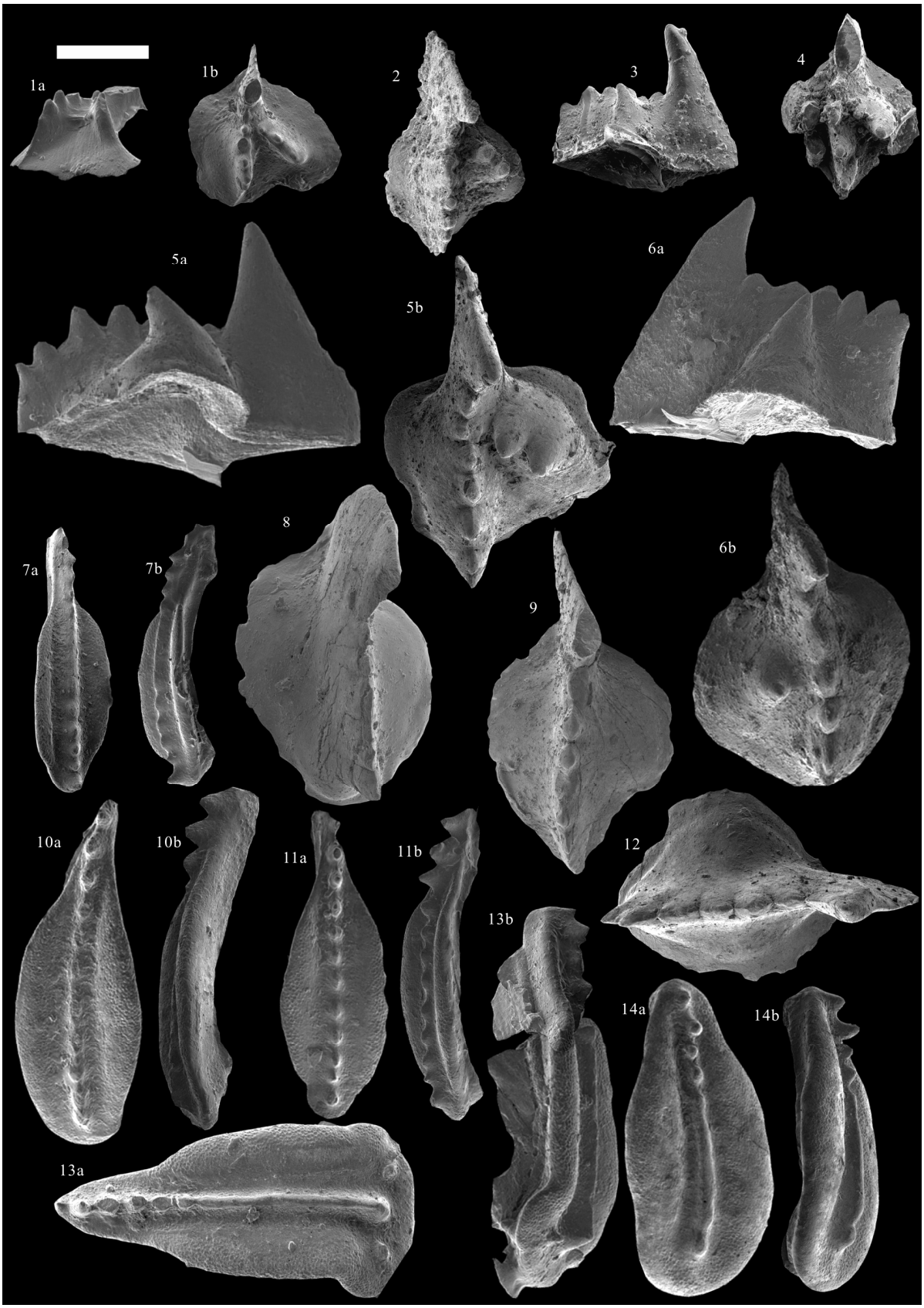

Plate 2. P_1 elements from the Dala Section. Scale bar equals 200 μm. 1, 2, 3, 5, 6. *Isarcicella staeschei* Dai and Zhang, 1989; Bed 17, DAL-15, 1. lateral view and upper view; 2. upper view; 3. lateral view; 5, 6. lateral view and upper view. 4. *Isarcicella isarcica* (Huckriede, 1958); Bed 12, DAL-13, upper view. 7. *Clarkina* cf. *carinata*; Bed 17, DAL-15, lateral view and upper view. 8, 9, 12. *Isarcicella inflata* Perri and Farabegoli, 2003; Bed 15, DAL-14, upper view. 10. *Clarkina lehrmanni* Chen et al., 2009; Bed 17, DAL-15, lateral view and upper view. 11. *Clarkina carinata* (Clark, 1959); Bed 17, DAL-15, lateral view and upper view. 13. *Clarkina* sp.; Bed 17, DAL-15, lateral view and upper view. 14. *Clarkina planata* (Clark, 1959); Bed 17, DAL-15, lateral view and upper view.

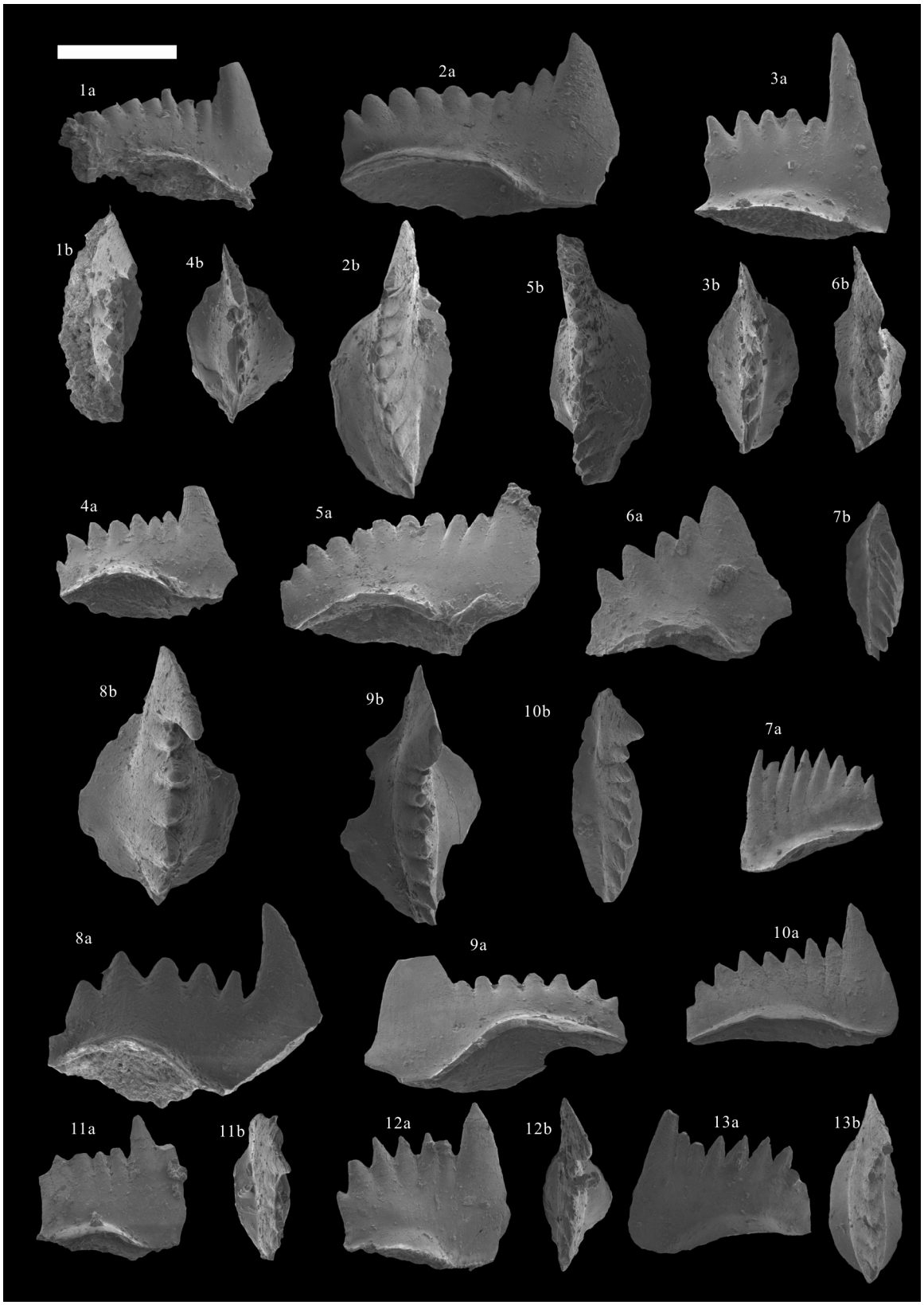

Plate 3. P_1 elements from the Dala Section. Scale bar equals 200 μm. 1. *Hindeodus* cf. *parvus*; Bed 10, DAL-6, lateral view and upper view. 2, 4, 5, 6, 7, 10. *Hindeodus praeparvus* Kozur, 1996; lateral view and upper view; 2. Bed 10, DAL-6; 4, 5. Bed 11, DAL-11; 6, 7. Bed 11, DAL-12; 10. Bed 12, DAL-15. 3, 11, 12. *Hindeodus parvus* (Kozur and Pjatakova, 1976); lateral view and upper view; 3. Bed 11, DAL-11; 11. Bed 11, DAL-12; 12. Bed 17, DAL-15. 8, 9. *Isarcicella turgida* (Kozur et al., 1975); lateral view and upper view; 8. Bed 11, DAL-12; 9. Bed 17, DAL-15. 13. *Isarcicella prisca* Kozur, 1995; lateral view and upper view; Bed 17, DAL-15.

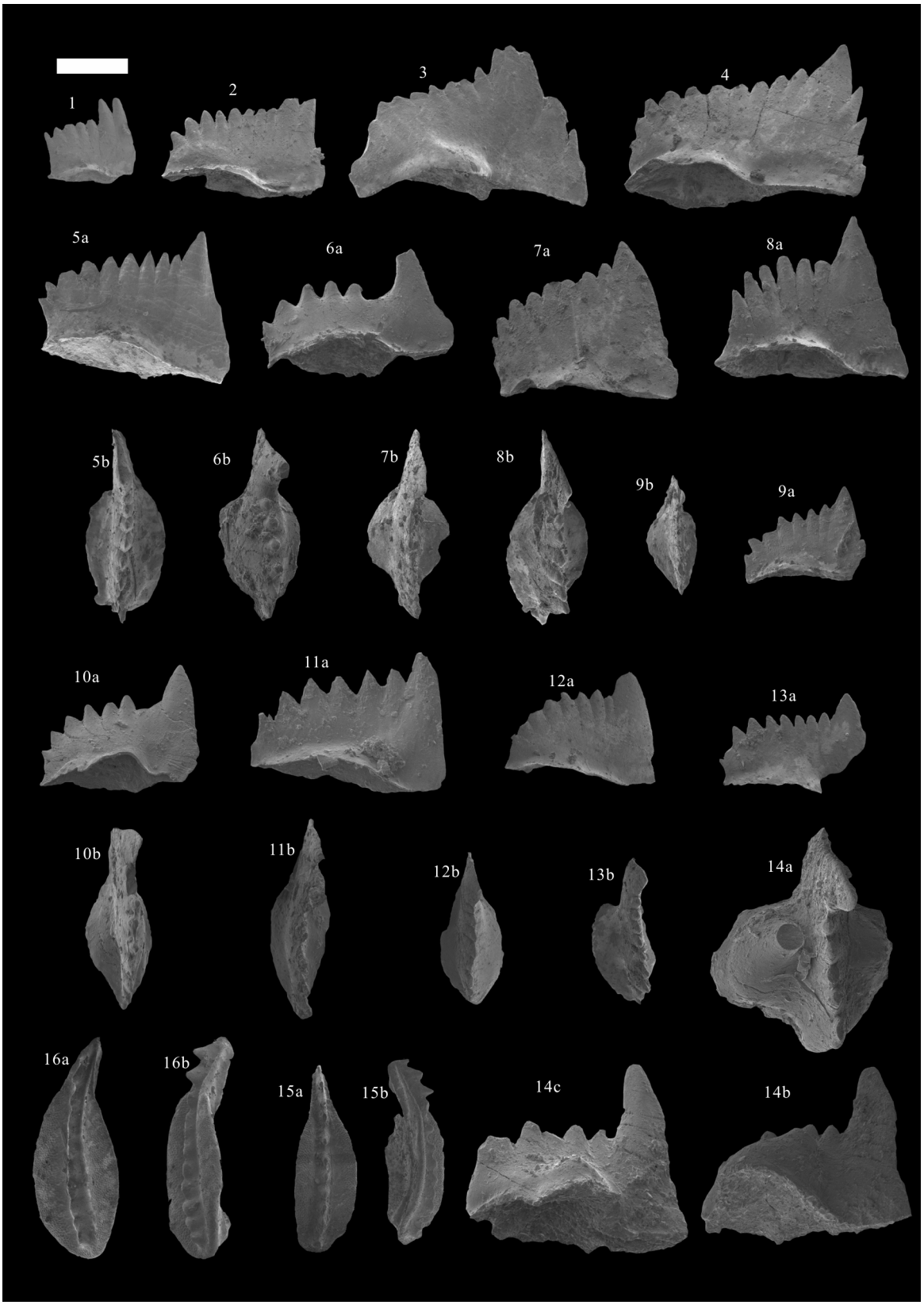

Plate 4. P_1 elements from the Dala Section. Scale bar equals 200 μm. 1, 4, 8, 13. *Hindeodus parvus* (Kozur and Pjatakova, 1976); 1, 4. Bed 17, DAL-15, lateral view; 8. Bed 17, DAL-17, lateral view and upper view; 13. Bed 17, DAL-18, lateral view and upper view. 2, 3. *Hindeodus peculiaris* (Perri and Farabegoli, 2003); Bed 17, DAL-15, lateral view. 5, 7, 9, 10, 11, 12. *Hindeodus praeparvus* Kozur, 1996; 5, 7, 9. Bed 17, DAL-17, lateral view and upper view; 10, 11, 12. Bed 17, DAL-18, lateral view and upper view. 6. *Isarcicella turgida* (Kozur et al., 1975); Bed 17, DAL-15, upper view and lateral view. 14. *Isarcicella staeschei* Dai and Zhang, 1989; Bed 17, DAL-15, upper view and lateral view. 15. *Clarkina taylorae* (Orchard et al., 1994); Bed 17, DAL-15, upper view and lateral view. 16.*Clarkina lehrmanni* Chen et al., 2009; Bed 17, DAL-15, upper view and lateral view.